Check for updates

Endonuclease-like activity of the N-terminal domain of *Euplotes octocarinatus* centrin†

Wenlong Zhang,[a] Enxian Shi,[ab] Yanan Feng,[a] Yaqin Zhao [iD][a] and Binsheng Yang [iD]*[a]

Euplotes octocarinatus centrin (EoCen) is a member of the EF-hand superfamily of calcium-binding proteins, which refer to nucleotide excision repair (NER). However, the role of centrin in NER is not clear. To explore the possible role of centrin, we initiated a physicochemical study of the N-terminal domain of *Euplotes octocarinatus* centrin (N-EoCen) with DNA in the absence or presence of Ca(II) in 10 mM Hepes at pH 7.4. N-EoCen shows unusual affinity for double-stranded DNA. The interaction results in the protein exposing more hydrophobic surface along with a certain perturbation taking place in the double helix structure. Interestingly, N-EoCen exhibits endonuclease-like activities *via* a hydrolysis pathway, which induces DNA strand breaks, such as supercoiled DNA into nicked circular and linear DNA. Importantly, mutation of serine (Ser) and threonine (Thr) to alanine (Ala) demonstrates that Ser and Thr, in particular Ser located at 22 (Ser22), may be the key residues responsible for DNA cleavage activity. The coordination of apoN-EoCen with Ca(II) can promote the binding to DNA and raise the cleavage activities. In contrast, the binding to Ca(II) of mutant proteins may trigger a conformational change so that the cleavage activity decreases dramatically, as confirmed by protein hydrolysis activity experiments. This is first report of the endonuclease-like activity of centrin, which provides valuable information for understanding a novel property of centrin, as well as knowledge of the functional diversity of centrin.

1 Introduction

Interaction between protein and nucleic acid is the basis of cell life, which relates to lots of crucial processes consisting of the regulation of gene expression, DNA replication and repair.[1,2] Many techniques have been developed for the mapping of DNA–protein interaction.[3–6] The interaction between protein and DNA involves van der Waals, hydrogen bonding, electrostatic and water-mediated interactions.[7] Most of the interactions are nonspecific and related to the sugar-phosphate backbone of DNA,[8] which provides stability to enhance the specific association rate by initially binding to DNA anywhere followed by intramolecular translocation to the specific binding site.[9] For example, non-specific protein–DNA interactions control I-CreI target binding and cleavage.[10] Sometimes specific base sequences also take part in the interactions. One classical example is Fe(II)-Fur, Fe(II)-dependent ferric uptake regulator, dimerizes and then binds to the specific sequence to repress gene transcription.[11] Thus, nonspecific protein–DNA interaction is a critical intermediate step in the process of sequence-specific recognition and binding.[12] Nonspecific reactions

generally refer to a highly dynamic process, which the protein can bind to and readily move between multiple binding sites on the DNA.[13]

Centrins are small, highly conserved members of the EF-hand superfamily of calcium-binding proteins that are found throughout eukaryotes.[14] They are related to the Ca(II)-binding protein, calmodulin, their common structural and functional unit is the EF-hand motif. Ca(II) sensor EF-hand domains change conformation upon Ca(II) binding, from a closed to an open form.

The protein is mostly concentrated in the microtubule-organizing centers (MTOCs), functionally related to the regulation of the MTOC duplication, separation during the cell cycle, and the nuclear mRNA export machinery in yeast.[15,16] Similarly with calmodulin being a calcium signal protein, a general view of how centrin works is that the binding of calcium facilitates target peptide recognition by the protein, with low-affinity peptide binding sites becoming activated in the presence of calcium, as in the case of *Scherffelia dubia* centrin.[17] Moreover, the literature have suggested that dubia centrin forms extended filamentous structures in a calcium-dependent manner.[17] Besides, calcium-binding capacity of centrin is required for linear POC5 assembly.[18] Despite sharing similarity with calmodulins, centrin has mass different properties, such as self-assembly based on a disordered region of first 20 amino acids.[19] Interestingly, aside from the roles of centrin in ciliogenesis and possible functions in centriole

[a]*Key Laboratory of Chemical Biology and Molecular Engineering of Ministry of Education, Insitute of Molecular Science, Taiyuan 030006, China. E-mail: yangbs@sxu.edu.cn; Tel: +86-351-7016358*

[b]*Department of Pharmacy, Shanxi Medical University, Taiyuan 030006, China*

activities, there are several emerging questions on its functions in DNA repair. It was found that only 10% of the total centrin is localized in MTOCs.[20] Centrin defective *Arabidopsis* plants are hypersensitive to UV-C and exhibit a reduced efficiency of DNA synthesis-dependent repair of UV induced DNA damage.[21] Centrin-defcient cells of vertebrate are markedly sensitive to UV irradiation and require centrin for effcient DNA repair.[22] centrin interacts directly with XP group C responsible gene product (XPC), and that centrin, in cooperation with human homologue of Rad23B (HR23B), stabilizes XPC, which stimulates NER activity *in vitro*.[23–25] Namely. They are localised appropriately to the sites of DNA damage by XPC and in turn control XPC stability and function. These findings implicate centrins in a recognition process in NER away from the centrosome. However, the research about centrin-DNA direct interactions remain lacking. Understanding of centrin functions, and particularly the Ca(II) dependence,[26] requires a detailed description of the molecular and structural properties of the isolated proteins and of their interactions with relevant cellular targets.

N-Terminal domain of *Ciliate Euplotes octocarinatus* centrin (N-EoCen), containing a pair of EF-hands referred to as site I and site II of 101 residues,[27] exhibits a more compact conformation. N-EoCen can bind two Ca(II) with moderate affinity.[27,28] The protein has three tyrosines (Tyr), located at position 46, 72, 79 respectively, which are considered as intrinsic fluorescence probes to monitor protein conformational changes, and intermolecular interactions. We therefore initiated a molecular and thermodynamic research aimed to determine the detailed N-EoCen and DNA binding parameters and Ca(II)-dependent functional properties of the N-EoCen.

In the present work, the N-EoCen–DNA complexes were examined by spectroscopy, polyacrylamide gel electrophoresis (native-PAGE), isothermal titration calorimetry (ITC) and DNA cleavage experiments. The data showed that N-EoCen binds to DNA with moderate affinities, and that it can cleave DNA in the absence or presence of Ca(II).

2 Experimental

2.1 Materials

4-(2-Hydroxyethyl)-1-piperazineethanesulfonic acid (Hepes), 2,6-*p*-toluidinonaphthalene sulfonate (TNS), bromophenol blue, Coomassie brilliant blue R-250, pBR322 DNA and calf thymus DNA (CT-DNA) were purchased from Sigma. The chemicals and the proteins are of the highest commercially available purity. Ethidium bromide (EB) was from Molecular Probes and 4-nitrophenyl acetate (4NPA) from acros organics. Calcium chloride (CaCl$_2$) was purchased from Sangon Biotech from Shanghai in China. The solution of TNS was prepared by dissolving weighed samples. In this study, we considered the concentration of base pairs (bp) of the DNA to be the overall concentration of DNA excluding the calculation of binding constant studies where the concentration of DNA was estimating by the concentration of base pairs divided by 1402 (GenBank: J00037.1). The filtered DNA solution gave an ultraviolet (UV) absorbance ratio (A_{260}/A_{280}) of 1.92, indicating that

DNA was sufficiently free from protein.[29] The concentration of bp was determined from the absorption at 260 nm ($\varepsilon_{260} = 6600$ M^{-1} cm^{-1}, $T = 298$ K). All experiments were carried out in Hepes buffer at pH 7.4. Protein preparation and the measurement of protein concentration were detailed in our previous work.[27] SA N-EoCen gene which Ser (serine) located at 22 and 43 are replaced by Ala (alanine), TA N-EoCen gene which Thr (threonine) located at 38, 41 and 90 are replaced by Ala, and STA N-EoCen gene which all Ser and Thr are replaced by Ala were synthesized by Sangon Biotech in Shanghai of China. The mutation proteins were confirmed by DNA sequencing assay. Mutation proteins were expressed and purified using the same procedure as that for apoN-EoCen.

2.2 CD measurements

CD measurements were performed with an MOS 450 (BioLogic, France) spectropolarimeter. All spectra were the average of three scans with a step size of 0.2 nm and a band width of 1 nm. CD spectra were recorded between 200 and 320 nm using 1 cm path length quartz cells. All experiments were done at room temperature in Hepes (pH 7.4).

2.3 Native polyacrylamide gel electrophoresis (native-PAGE)

Different concentrations of CT-DNA, N-EoCen and 2 mM Ca(II) (only the reaction was performed in the presence of Ca(II)) were incubated in Hepes (10 mM, pH 7.4), at 4 °C for 12 h. Then loading buffer (1/5 volume) consisting of 50% glycerol, 0.5% bromophenol blue, was supplemented to the sample completed before electrophoresis. Samples were analyzed in 15% native polyacrylamide gel (acrylamide/bis-acrylamide = 29 : 1) containing tris-glycine buffer at the constant potential 80 V. Positions of protein was visualized by staining with Coomassie brilliant blue R-250 staining solution (0.25% Coomassie brilliant blue R-250, 45% methyl alcohol, 10% glacial acetic acid) using ZHGP-70I film illuminator from ProteinSimple.

2.4 Fluorescence lifetime and time-resolved anisotropy

Fluorescence lifetimes and time-resolved anisotropy decays measurements were detailed in previous work.[30] Fluorescence decays, $I(t)$, were measured in 10 mM Hepes, pH 7.4, at 25 °C. The excitation wavelength and emission wavelength are 280 nm and 306 nm, respectively. The fluorescence decay of Tyr was analyzed using a sum of exponentials: $I(t) = \sum B_i \exp(-t/\tau_i)$, where B_i and τ_i are the amplitude and lifetime, respectively.

2.5 DNA melting

DNA melting experiments were performed in 1 cm quartz cells using a Varian-Cary Eclipes UV-Vis spectrophotometer. Samples were continuously heated with a 5 °C interval of temperature increase while monitoring the absorbance changes at 260 nm. The investigated interval of temperature ranged from 5 to 90 °C.

2.6 Spectrofluorimetric methods

Steady-state emission of TNS and EB were measured with a Varian-Cary Eclipse fluorescence and HORIBA Scientific

Fluoromax-4 spectrometer, respectively. The protein and CT-DNA mixed solution was equilibrated for 10 min before addition of TNS or EB. The excitation wavelength was set at 320 nm for TNS and 488 nm for EB. The excitation and emission slits were both 5 nm. In the fluorescence titrations experiments, the DNA binding affinity for N-EoCen was measured by monitoring the fluorescence intensity of Tyr. The fluorimetric titrations experiments were carried out in Hepes (pH 7.4) by keeping the concentration of N-EoCen as constant (10 μM) and varying the concentration of CT-DNA (0–0.45 mM). The protein and CT-DNA mixed solution was equilibrated for 10 min. Spectra were collected on a Cary Eclipse spectrofluorimeter, with excitation at 280 nm. Emission was recorded in the range from 285 to 500 nm. The excitation and emission slits were both 10 nm. Binding constant (K_a) and binding stoichiometry (n) of the CT-DNA to N-EoCen was determined from the eqn (1)

$$\log \frac{F_0 - F}{F} = \log K_a + n \log[Q] \tag{1}$$

where F_0 and F are the fluorescence intensities of N-EoCen in the absence and the presence of CT-DNA, respectively. [Q] is concentration of quencher (CT-DNA). From the plot of $\log[(F_0 - F)/F]$ versus $\log[Q]$, the number of binding sites n and K_a are obtained.[31,32]

2.7 ITC titrations

ITC experiments were performed at 298 K using a MicroCal ITC200 device (GE Healthcare Life Sciences). The instrument consists of one sample cell and one reference cell. The reference cell was filled with ultrapure water. 300 μL of protein solution (0.06 mM) was deposited in the sample cell during a typical titration, with stirring at 750 rpm. 1 μL of CT-DNA solution (0.8 mM) was injected at equal 300 s intervals into sample cell (0.4 μL on the first injection). In total, 30.4 μL of CT-DNA solution was added to protein solution. The heat effects due to dilution and mixing were assessed by injecting CT-DNA solution into buffer under the same conditions, and these values were subtracted from the effects produced by the CT-DNA–protein interaction. The heat released by dilution of protein was little and thus neglected. Calorimetric analyses were carried out with "one set of sites" of the Origin™ fitting package.

2.8 Cleavage of pBR322 DNA

The cleavage reaction of pBR322 DNA was carried out in the mixture containing 0.025 μg μL^{-1} of plasmid in 10 mM Hepes buffer (pH 7.4) with various concentrations of proteins. Total reaction volume was 20 μL. Samples were incubated for 2 h unless otherwise stated at room temperature. Soon afterwards, all samples were loaded on the 1% agarose gel, containing 4S Green Plus Nucleic Acid Stain. Electrophoresis was carried out at 110 V in 1× TAE (Tris–acetic–EDTA) buffer. Supercoiled DNA cleavage products, which were visible as bands on the agarose gel, were quantified and analyzed with Alpha Imager. The efficiency of the DNA cleavage was assessed by determining the ability of the species from the supercoiled form (Form I) to nick circular from (Form II) or linear forms (Form III), by

quantitatively estimating the intensities of appropriate bands using the GeneTools software (Alpha Imager).

Additionally to standard conditions of pBR322 DNA cleavage, some reactions were performed in the presence of several inhibitors, which were included into reaction mixture before apoN-EoCen addition.

2.9 T4-ligase religation assay

The nicked circular and liner forms of pBR322DNA cleavage products by apoN-EoCen and endonuclease BamH I were isolated and purified using Easypure quick Gel Extraction Kit (TransGen biotech). Then the isolated DNA cleavage products were incubated with T4-ligase and ligation buffer for 15 h at 16 °C for ligation reaction. Afterwards, the ligation products were electrophoresed, stained and imaged.

2.10 Hydrolysis activity assay

The hydrolysis activities of different protein were evaluated by using 4-nitrophenyl acetate (4NPA) as a substrate. Kinetic experiments were initiated by the addition of 4NPA to a solution containing 5 μM protein in 10 mM Tris–HCl (pH 7.0) at 25 °C. The hydrolysis product of 4-nitrophenoxide was monitored by absorption increase at 400 nm with a Varian-Cary Eclipes UV-Vis spectrophotometer. Spontaneous hydrolysis of 4NPA was also monitored in 10 mM pH 7.0 Tris–HCl buffer. The initial rates were determined from linear fits of the absorbance versus time and observed rate constants (k_{obs}) calculated using an extinction coefficient of $\varepsilon_{400} = 18.3$ mM^{-1} cm^{-1} (ref. 33–35) and protein concentration. The kinetic parameters (k_{cat} and K_m) were determined by fitting the curves of k_{obs} versus the concentration of 4NPA to the Michaelis–Menten eqn (2)[36]

$$k_{obs} = \frac{k_{cat} \cdot [\text{4NPA}]}{K_m + [\text{4NPA}]} \tag{2}$$

It was revised by the spontaneous hydrolysis of 4NPA.

2.11 Molecular docking studies

All docking studies were carried out with ZDOCK 3.0.2 (http://zdock.umassmed.edu).[37–39] The crystal structures of DNA duplex (PDB:2k0v), apoN-EoCen (PDB:2joj) and modeled holoN-EoCen were obtained from PDB. Prediction of possible complexes using the server proceeds in three steps. Firstly, on the initial submission page, users provide two input structures to be docked. The next step is selection of residues for each submitted crystal structures, which is aided by JMol visualization of each molecule that highlights selected residues for the user. Finally, a link to the results is emailed to users.

2.12 Statistical analysis

All experiments were performed in triplicate ($n = 3$) to ensure accuracy and reliability of the results. In the quantitative evaluations, the results were presented considering the mean value and the respective standard deviation (SD) of three independent experiments. The linear regression analyses for eqn (1) and (2)

were performed at a 96% confidence interval using the software Sigma Plot 10.0.

3   Results and discussion

3.1   Binding of N-EoCen and DNA

3.1.1   Circular dichroism (CD) spectroscopy. DNA binding is a critical step for subsequent cleavage. Hence, prior to research the cleavage activities of N-EoCen, the binding properties of N-EoCen with CT-DNA were monitored using various methods.

CD provides a rather convenient method for the determination of the structural changes environmentally induced in proteins based on the different forms of the primary secondary structural elements found in proteins (*e.g.*, α-helix, β-sheet, and random loop).[40] In order to investigate the interactions and any structural perturbation of the N-EoCen with CT-DNA, the CD spectroscopy was monitored. As seen from Fig. 1A, apoN-EoCen exhibits a negative CD signal at 222 nm, which is commonly used as quantifying α-helix of protein. In addition, CT-DNA in buffer (Fig. 1B), displays a negative CD signal at 244 nm and a positive CD signal at 277 nm that is characteristic of B-DNA structure.[41] Upon mixing the two solutions, a dramatic difference in the shape and intensity between the subtraction spectra and single-component spectra is observed. In Fig. 1A, a drastic decrease is detected after addition CT-DNA into protein even if the CD profiles of apoN-EoCen in buffer remains essentially similar to that in the presence of CT-DNA. It suggests that a significant conformation change of protein induced by CT-DNA happens. Simultaneously, a strong variation of the CD profile of CT-DNA is displayed (Fig. 1B). In more detail, the negative peak at 244 nm shifts to 247 nm while the negative band becomes narrow, and the positive peak enhances in the presence of apoN-EoCen, suggesting that double helix structure changes a lot associated with the protein–DNA complex formation.

Based on our previous reports, the coordination with Ca(II) has less effects on the α-helix of apoN-EoCen,[42] as seen in Fig. 1C. A slight increase in molar ellipticity at 222 nm is indicated after addition of Ca(II) into apoN-EoCen. Similarly to apoN-EoCen, holoN-EoCen also shows reduced α-helix content than that of holoN-EoCen alone, upon addition of CT-DNA (Fig. 1C). For CT-DNA in the presence of holoN-EoCen (Fig. 1D), the negative peak (244 nm) shifts as well as the band narrows. Beyond that, the positive band of DNA at 277 nm weakens after holoN-EoCen-CT–DNA complex formation, which may attribute to the binding of Ca(II) to CT-DNA. Therefore, we reasons that holoN-EoCen can also react with CT-DNA.

3.1.2   Native-PAGE analysis. To further evaluate the perturbation of protein structure due to the interactions, native-PAGE was performed, as shown in Fig. 1E and F. By contrasting with the low concentration of N-EoCen (lane 1), the high concentration of protein appears different (lane 2). The relative high concentration of protein appears multimer (lane 2, upper band) compared with the protein with low concentration, only monomer (lane 1). Both apoN-EoCen and holoN-EoCen, the level of monomer increasing and multimer reducing of proteins

with gradually increasing concentration of CT-DNA is represented. It has been reported that the aggregation of proteins mainly depends on hydrophobic effect, and the Tyr at position 79 may play a critical role in the process by our earlier research.[43,44] Taking into account all these considerations, the transformation from multimer to monomer of protein uncovers that the protein–protein interactions suffers from inhibition probably through steric effect, and the microenvironment of Tyr 79 of N-EoCen changes much resulted from the binding of protein and DNA. Namely, the binding to the DNA is not in favour of the aggregation of proteins. Compared with that of apoN-EoCen (lane 6 in Fig. 1E), the multimer of holoN-EoCen disappears at the lower concentration of CT-DNA (lane 5 in Fig. 1F). In fact, holoN-EoCen is easy to aggregate.[43] It seems that the conformational change of protein induced by Ca(II) may facilitate the interaction between protein and DNA.

3.1.3   Fluorescence lifetime and time-resolved anisotropy. Fluorescence lifetimes of apoN-EoCen, holoN-EoCen and the complexes with CT-DNA were exploited to further detect the local environment change of Tyr in protein, and the results were presented in Fig. 2A and B. It can easily be seen that the lifetime of Tyr in N-EoCen changes in the presence of different solutions. The decays are found to be multiexponential in nature with two decay components (τ_i) and the lifetimes are listed in Table 1. For apoN-EoCen (Fig. 2A), the overall fluorescence decay leads to an average decay time ($\Sigma \tau_i B_i$) constant of (1.84 ± 0.01) ns. The fluorescence transient of the apoN-EoCen–CT-DNA complex (average decay time of (0.89 ± 0.02) ns) is found to be slower nearly 52% than that of the apoN-EoCen emission. The slower fluorescence decay is probably a consequence of that the binding of CT-DNA with protein changes the microenvironment of Tyr,[45] which matches the native-PAGE results. Those observations suggest strongly that the interaction between the CT-DNA and apoN-EoCen has a comparatively effect on the conformation of apoN-EoCen.

Just as the combination of calmodulin with calcium leads to α-helix orientation change and hydrophobic residues exposing to the solvent, holoN-EoCen also undergoes conformation change.[46,47] As shown in the Table 1, the fluorescence average decay time of holoN-EoCen is (2.23 ± 0.01) ns. Upon adding to CT-DNA, the fluorescence average decay time of holoN-EoCen ((0.98 ± 0.03) ns) decreases by 56% (Fig. 2B), demonstrating that the local environment of Tyr in holoN-EoCen bound with CT-DNA changes more.

To further elucidate the interaction of protein and DNA, the fluorescence anisotropy was monitored. As shown in Fig. 2C, apoN-EoCen in the presence of CT-DNA has a relatively higher initial anisotropy value (0.051 ± 0.002) compared with that of apoN-EoCen (0.021 ± 0.001), reflecting that the considerable interaction of the protein with CT-DNA leads to the Tyr in protein not to easily rotation. As for holoN-EoCen–DNA complex, Tyr residue in protein also shows reduced rotational freedom (Fig. 2D).

3.1.4   Hydrophobic packet changes of N-EoCen induced by CT-DNA. TNS is widely used as a biological probe to detect the exposed hydrophobic surface based on hydrophobic interaction between it and apolarity regions of protein structure.[48]
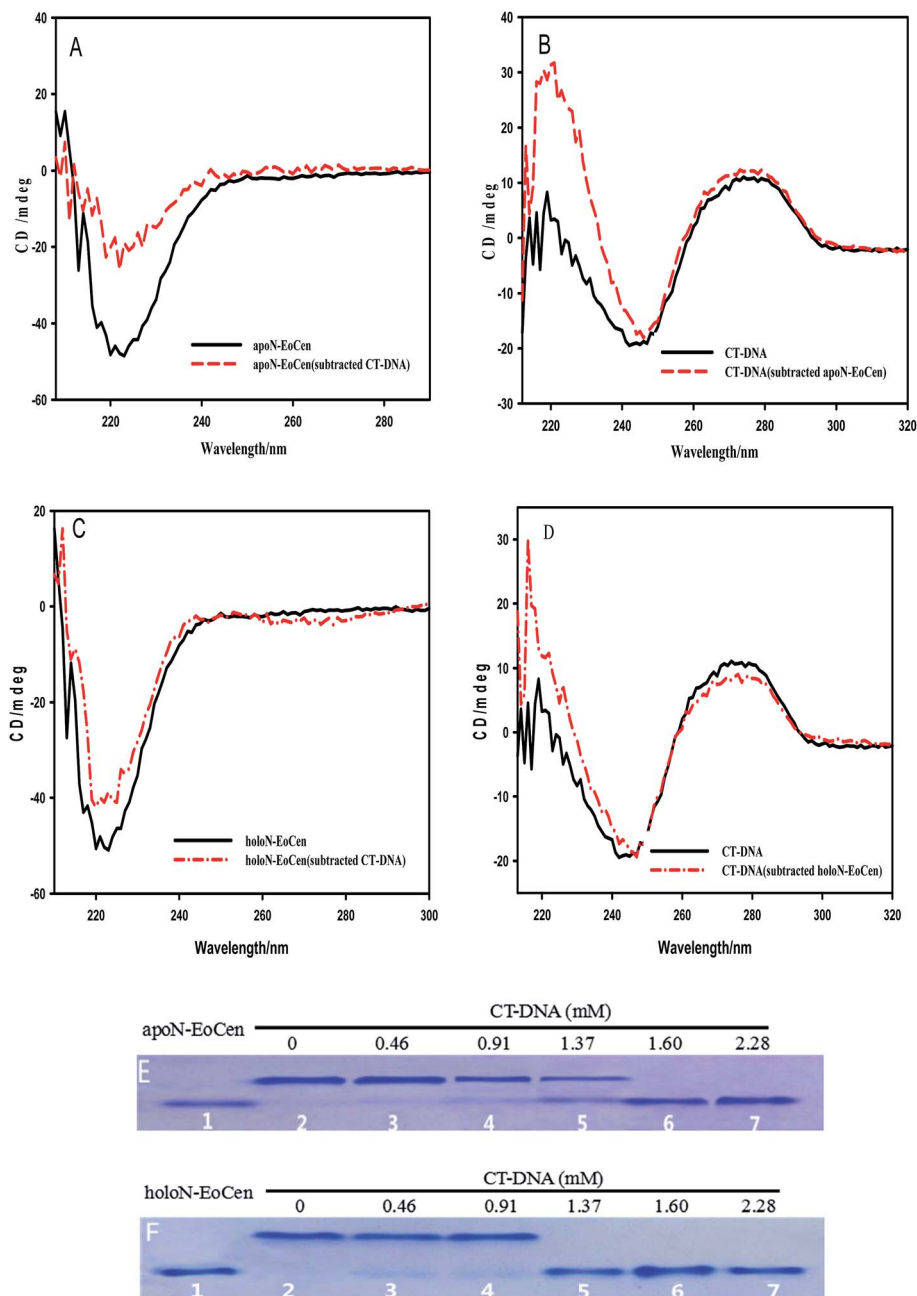
Fig. 1 N-EoCen binds to CT-DNA. (A) CD spectrum of apoN-EoCen (4.56 μM), measured or obtained by subtraction of the DNA spectrum from that of apoN-EoCen-DNA complex. (B) CD spectrum of DNA ([bp] = 0.16 mM), measured or obtained by subtraction of the apoN-EoCen spectrum from that of apoN-EoCen–DNA complex. (C) CD spectrum of holoN-EoCen (4.56 μM, [Ca^{2+}] = 2 mM), measured or obtained by subtraction of the DNA spectrum from that of holoN-EoCen–DNA complex. (D) CD spectrum of DNA, measured or obtained by subtraction of the holoN-EoCen spectrum from that of holoN-EoCen–DNA complex. (E) Native-PAGE of apoN-EoCen (45.6 μM) with varying amounts of base pair (0, 0.46, 0.91, 1.37, 1.60 and 2.28 mM) corresponding to lane 2–7 after 12 h incubation at 4 °C and lane 1 N-EoCen (16.7 μM). (F) Native-PAGE of holoN-EoCen (45.6 μM) with varying amounts of base pair (0, 0.46, 0.91, 1.37, 1.60 and 2.28 mM) corresponding to lane 2–7 after 12 h incubation at 4 °C and lane 1 N-EoCen (16.7 μM).

Experiments have verified that N-EoCen has a high affinity for TNS.[45] As seen in Fig. S1a,† the emission intensity of TNS is fairly small in Hepes (10 mM, pH 7.4) or in CT-DNA solution with an emission maximum at 506 nm. Strikingly, the TNS-apoN-EoCen solution displays a large relative fluorescence intensity together with a blue shift of 54 nm compared to that in

buffer as a result of the attachment of TNS to the protein (452 nm). Upon addition of CT-DNA to TNS-apoN-EoCen solution, a considerable increase in the fluorescence intensity, together with a peak shift to the blue by 23 nm (from 452 nm in TNS-apoN-EoCen to 429 nm in TNS-apoN-EoCen–CT-DNA) is found. The changes owe to that the complexation between
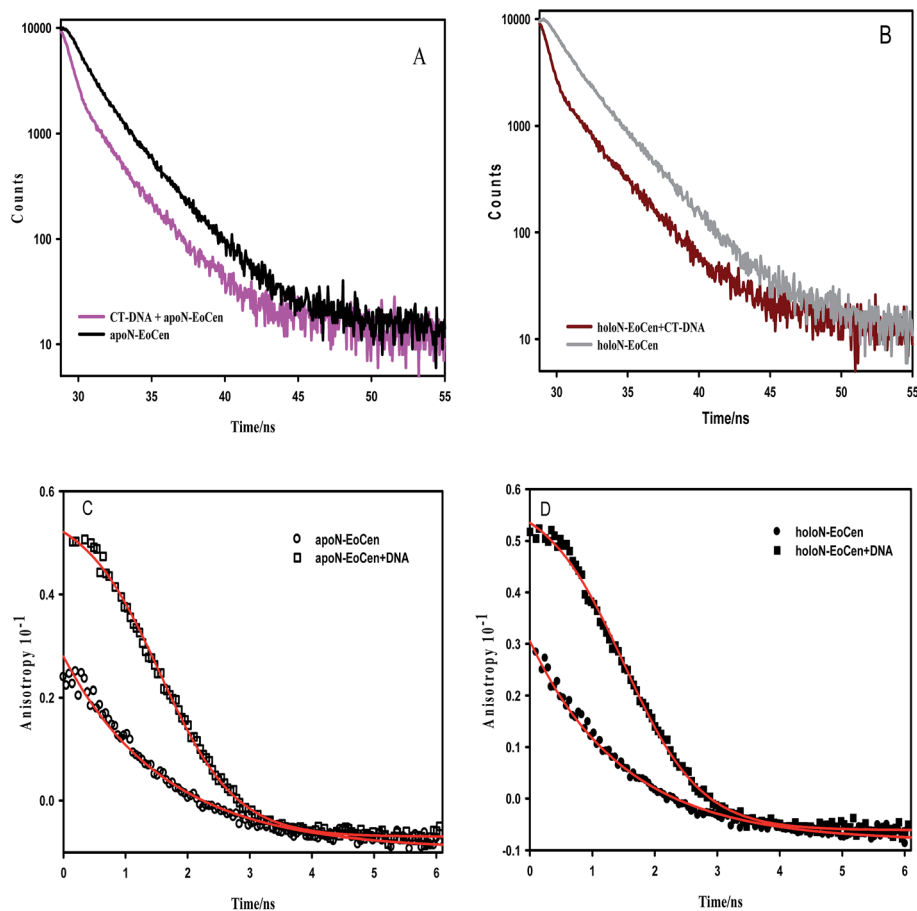
Fig. 2 Microenvironment change of Tyr of protein after interaction with CT-DNA. Fluorescence decay curves of apoN-EoCen (10 μM) (A) and holoN-EoCen (10 μM, $[Ca^{2+}]$ = 2 mM) (B) in the absence or presence of CT-DNA ([bp] = 0.35 mM) in 10 mM Hepes buffer (pH 7.4) at room temperature. Fluorescence anisotropy decays of apoN-EoCen (10 μM) (C) or holoN-EoCen (10 μM, $[Ca^{2+}]$ = 2 mM) (D) in the absence or presence of CT-DNA ([bp] = 0.35 mM) in 10 mM Hepes buffer (pH 7.4) at room temperature. Curves were recorded after the reaction mixture was incubated for 10 min.

CT-DNA and apoN-EoCen can facilitate apoN-EoCen to exposure more hydrophobic surface which TNS better combines to. It is consistent with the fluorescence lifetime measurements.

In Fig. S1b,† TNS fluorescence intensity increases more in the presence of holoN-EoCen than that of apoN-EoCen, which is in accordance with the early report.[45] In other words, holoN-EoCen can expose more hydrophobic surface. CT-DNA–holoN-EoCen exhibits significant enhancement in TNS fluorescence intensity, which reveals that more hydrophobic surface is exposed because of DNA binding to holoN-EoCen. In brief, the interaction with DNA leads to holoN-EoCen unfolding more

hydrophobic surface. It is may originated from that the open conformation induced by Ca(II) is closely related to the interaction of protein and DNA.

3.1.5 DNA melting. Another strong evidence for the interaction of N-EoCen with CT-DNA was acquired from the DNA melting studies. The melting temperature (T_m) is the temperature at which 50% of double stranded DNA becomes single stranded.[49] The absorbency of DNA bases at 260 nm in the double-helical form is much less than that in the single stranded form. DNA melting experiments were carried out by controlling various temperatures in the absence or presence of

Table 1 Fluorescence parameters of the interaction of N-EoCen with CT-DNA[a]

	τ_1 (%)	τ_2 (%)	$\langle\tau\rangle$
apoN-EoCen	1.08 ± 0.02 (51.28%)	2.64 ± 0.03 (48.72%)	1.84 ± 0.01
apoN-EoCen–CT-DNA	0.35 ± 0.02 (57.83%)	1.80 ± 0.04 (38.24%)	0.89 ± 0.02
holoN-EoCen	1.19 ± 0.04 (34.60%)	2.78 ± 0.02 (65.40%)	2.23 ± 0.01
holoN-EoCen + CT-DNA	0.31 ± 0.01 (56.43%)	2.15 ± 0.07 (37.25%)	0.98 ± 0.03

[a] B_i, τ_i and $\langle\tau\rangle$ are the amplitude (refer to the in parenthesis), lifetime and average lifetime, respectively.

apoN-EoCen or holoN-EoCen while monitoring the absorbance at 260 nm. As clearly seen in Fig. 3A and B, T_m of CT-DNA is 61 °C under the experimental conditions. It decreases to 58 °C in the presence of apoN-EoCen. The results clearly support that the double helix structure becomes instable upon complexation with apoN-EoCen, which is in accordance with the results of CD spectroscopy. This may be due to that the acidic amino acids of protein bind to CT-DNA in its groove and weaken the H-bonds between DNA strands, thereby destabilizing the double helix.[50] It can be seen that T_m of CT-DNA increase by about 3 °C from 61 °C to 64 °C upon addition 9.12 μM Ca(II). It indicate that Ca(II) renders the DNA double helix more stable, as reported by literature.[51] Sigel A et al. pointed out that metal ions can form a diffuse ion atmosphere and provide exactly the necessary charge neutralization to DNA, further stabilizing DNA structure.[52] Nevertheless, the T_m of holoN-EoCen–CT-DNA (Fig. 3B) becomes 57 °C, decreasing by more than 7 °C than CT-DNA–Ca(II). Besides, the T_m of CT-DNA decreases by 3 °C in apoN-EoCen and 4 °C in holoN-EoCen, respectively. Namely, the effect of holoN-EoCen on the T_m of CT-DNA is larger than that of

apoN-EoCen on CT-DNA. It indicates that the coordination with Ca(II) makes DNA easier be melted by holoN-EoCen.

3.1.6 Competitive with ethidium bromide (EB). In order to get more insight into the interaction mode of CT-DNA towards N-EoCen, the EB fluorescence titration experiments were performed. EB is widely used to describe the interaction of compounds with DNA by monitoring the changes of its fluorescence intensity.[53] As depicted in Fig. 3C, the intrinsic fluorescence intensity of EB in buffer is relative low, even though in the presence of protein. The fluorescence intensity of EB enhances when it intercalates into the DNA double helix. Nevertheless, the fluorescence intensity of DNA–EB system shows a markedly decreasing trend in the presence of apoN-EoCen. The loss of fluorescence intensity can be caused by the binding apoN-EoCen to DNA. Then it leads to the conformation change of DNA so that few EB molecules are released from DNA. The fluorescence intensity of Ca(II)–CT-DNA–EB (Fig. 3D) is much stronger than that of DNA–EB. Indeed, Ca(II) has stabilizing roles in DNA, and can be responsible for large conformational changes, such as inducing bending,[51] which
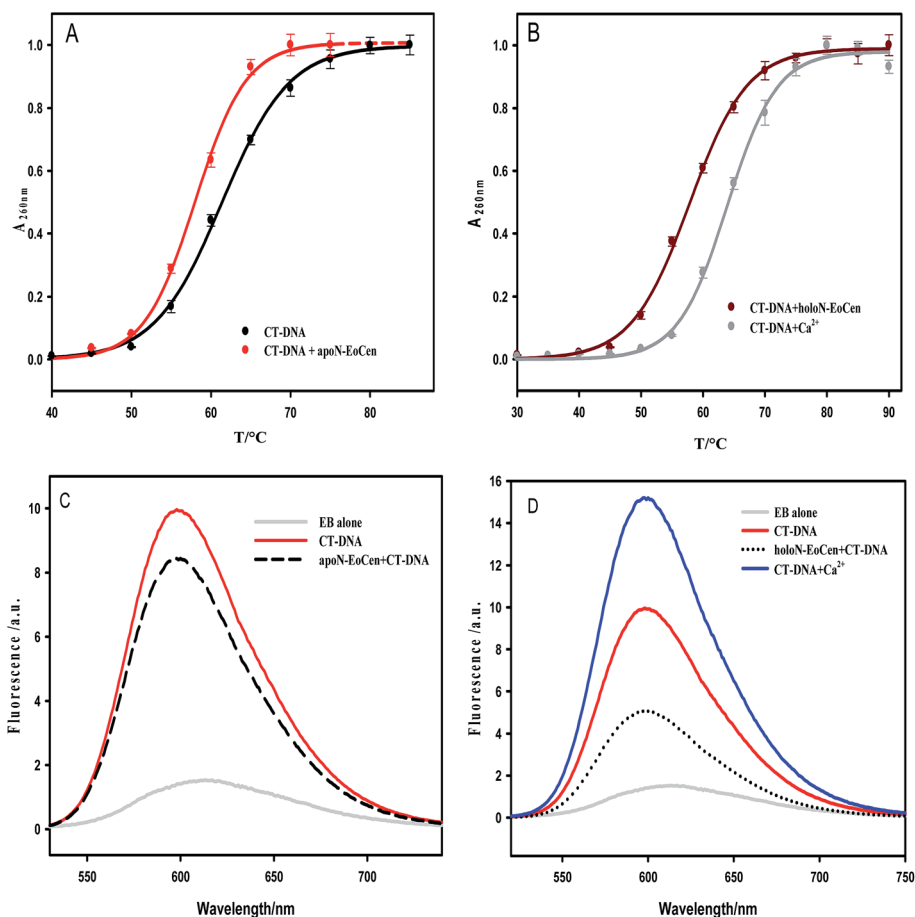
Fig. 3 The structure perturbation of CT-DNA after incubation with protein. Normalization of thermal denaturation curves (monitored at 260 nm) of CT-DNA ([bp] = 0.16 mM, T_m = 61 °C) in the absence and presence of apoN-EoCen (4.56 μM, T_m = 58 °C) (A) or holoN-EoCen (4.56 μM, T_m = 57 °C) (B), as well as a mixture of CT-DNA with Ca^{2+} (9.12 μM, T_m = 64 °C) (B). Steady-state fluorescence spectra of EB–CT-DNA ([bp] = 0.16 mM) in the presence of apoN-EoCen (4.56 μM) (C) or holoN-EoCen (4.56 μM, [Ca^{2+}] = 2 mM) (D), the spectra of EB in buffer and CT-DNA–Ca^{2+} were shown in (D), the concentration of EB was 0.85 μM. The spectra were recorded after the reaction mixture was incubated 10 min. Each assay was performed in three independent replicates, and values shown are means with SD.

may be good for binding of it with EB. The fluorescence intensity of holoN-EoCen–CT-DNA–EB (Fig. 3D) is even weaker than that of the apoN-EoCen–CT-DNA–EB complex. In consideration of the coordinate behavior of Ca(II), it cannot combine with protein and DNA at the same time. Hence the relatively weak fluorescence intensity of holoN-EoCen–CT-DNA–EB probably seems to stem from that the great conformational change of DNA bound with holoN-EoCen goes against the intercalating of EB. In other words, the coordination of Ca(II) with apoN-EoCen can promote the interaction between protein and DNA and subsequently may significantly influence the conformation of DNA.

3.1.7 Spectrofluorimetric titrations.

To gain further insight into the binding properties of N-EoCen and CT-DNA, steady-state fluorescence spectra were recorded. As revealed by Fig. S2a,† fluorescence emission maximum peak of apoN-EoCen shows slight redshift 6 nm from 306 nm (λ_{ex} = 280 nm) to 312 nm and quenching, with addition of CT-DNA, which corresponds to the microenvironment change around Tyr.[43,54] These changes may be attributed to binding of apoN-EoCen with the duplex, which could involve hydrogen bonds of the oxygen or nitrogen atoms on the protein with DNA nucleobases.[55,56] Furthermore, the structure of DNA suffers from perturbation as suggested in CD and DNA melting experiments. Inset of Fig. S2a† presents the fluorescence intensity of apoN-EoCen at 306 nm as a function of concentration ratio of bp to apoN-EoCen. The plot clearly shows that the fluorescence intensity of apoN-EoCen at 306 nm gradually decreases from 0 to 35 of the concentration ratio, and approaches a unchanged value when the concentration ratio is larger than 35. It means that the protein binds to CT-DNA in occluded site size about 35 bp. In comparison, the titration of CT-DNA to holoN-EoCen was carried out at the same condition (Fig. S2b†). The addition of DNA to the solution of holoN-EoCen induces a sharply decrease in the fluorescence intensity at 306 nm. From the plot of fluorescence intensity at 306 nm vs. [bp]/[holoN-EoCen] (insert), the apparent occluded site size of protein to DNA is also about 35 bp.

For the purpose of further understanding the binding nature between protein and DNA, the binding constants were calculated by using eqn (1) and listed in Table 2. The most notable result is that holoN-EoCen binds CT-DNA with a binding constant of 2.48×10^6 M^{-1} at 298 K, about 8-fold tighter than that of apoN-EoCen. A plausible explanation is that the binding with Ca(II) render conformation of protein change from closed

to open, which exactly contribute to the binding of protein to DNA. One binding site suggests that one protein molecular can bind with one DNA molecular.

3.1.8 ITC titrations.

ITC measurements of CT-DNA binding to N-EoCen were carried out to evaluate the driven force of the interaction, as well as the binding constants. For the interaction, the binding isotherm was best described by "one set of sites" binding model. The binding constant obtained for CT-DNA binding to apoN-EoCen is 8.12×10^4 M^{-1} (Table 2). The enthalpy change associated with CT-DNA binding to apoN-EoCen was positive, indicative of an endothermic process (Fig. 4). The enthalpy contribution to the free energy of binding is small, and about one time less than the entropic term $T\Delta S$, calculated according to measured values of K and ΔH (Table 2). The binding of CT-DNA to apoN-EoCen is thus mainly driven by entropy change. For CT-DNA binding to holoN-EoCen, the binding constant (2.22×10^5 M^{-1}, Fig. 4) is three times larger than that CT-DNA binding to apoN-EoCen, indicating that a major conformational change induced by binding with Ca(II) noticeably strengthens the binding of DNA to protein. The binding site of about one suggests that either apoN-EoCen or holoN-EoCen molecular can bind with one DNA molecular. It is in good accordance with spectrofluorimetric analysis result (Table 2). The binding constants acquired by ITC titrations slightly differ from the results obtained by fluorescence spectroscopy. The differences may be because of differences in experimental conditions and a larger imprecision of the fit for ITC data.

Together, all results obtained in the present study confirm that the formation of a protein–DNA complex arises possibly as a result of the interaction between the amino acid residues on the protein with DNA. The binding process induces a larger conformation change, such as the hydrophobic cavity exposing of protein and distortion of DNA structure. Obviously, one protein molecular can bind with a DNA molecular, which refers to 35 bp. Additionally, the conformation change from closed to open can be a good explanation of the facilitated of holoN-EoCen to the binding protein and DNA.

3.2 Endonuclease-like activity of DNA

It is can be found that DNA can be cleaved by N-EoCen after longer time incubation, as shown in Fig. 5A. The supercoiled DNA (Form I, lower band in lane 1) breakage results in the formation of nicked circular DNA (Form II, upper band in lane

Table 2 Binding parameters and binding sites for the interaction of N-EoCen with CT-DNA

Protein	Temperature/K	K_a (M^{-1} × 10^5)	n	ΔG (kJ mol^{-1})	ΔH (kJ mol^{-1})	ΔS (kJ mol^{-1} K^{-1})
apoN-EoCen	298	2.79 ± 0.2^a	0.962 ± 0.05^a	−24.7	315	1.14
		0.812 ± 0.4^b	0.998 ± 0.03^b			
holoN-EoCen		24.8 ± 0.1^a	1.07 ± 0.01^a	−29.2	534	1.89
		2.22 ± 0.2^b	1.58 ± 0.01^b			

^{a} Data from spectrofluorimetric titrations. ^{b} Data from ITC titrations.

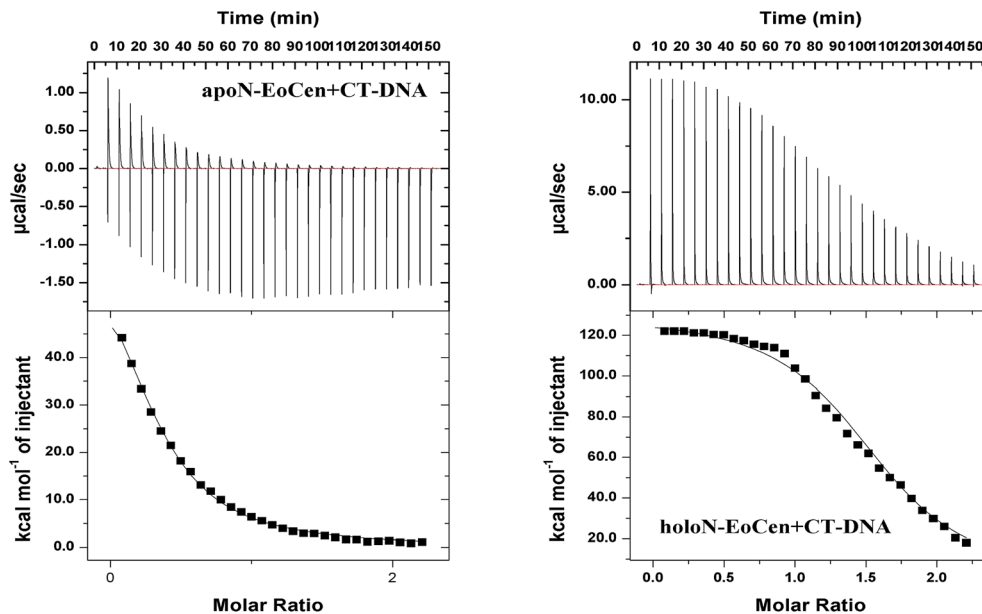**Fig. 4** ITC raw data and binding isotherm for CT-DNA interaction with N-EoCen in the absence or presence of Ca^{2+} at 298 K. Data points are the average of three experiments. Solid lines represent the best fit results according to a "one set of sites" model.

4) in the presence of apoN-EoCen. Linear DNA (Form III, middle band in lane 5) appears in the presence of holoN-EoCen. However, the nicked circular and linear DNA does not appear in the presence of human serum albumin (HSA) (lane 2) or metal ions (lane 3) under the similar conditions. Therefore, the conversion of the supercoiled to the nicked circular DNA and linear DNA exhibits that N-EoCen has endonuclease-like activity at physiological pH and room temperature. The cleavage capacity of holoN-EoCen is stronger than that of apoN-EoCen. This is first report of the endonuclease-like activity of the centrin, which may be closely related to its cellular functions in living creature. To further investigate the cleavage behaviors of N-EoCen, the gel electrophoresis experiments were performed.

3.2.1 Cleavage of supercoiled DNA. Fig. 5B and C present the agarose gel electrophoresis patterns for the cleavage of pBR322 DNA after 3 h treatment with apoN-EoCen or holoN-EoCen with various concentrations (from 0 to 28.6 μM), respectively. When pBR322 DNA was incubated with apoN-EoCen or holoN-EoCen, the Form I of the plasmid was cleaved to the Form II, a single nick circular of DNA strand, soon afterwards, supercoil structure of the plasmid gradually formed the Form III, a linear DNA strand. From the Fig. 5B and C, we can conclude that the cleavage efficiency of N-EoCen appears when the protein concentration is up to 0.286 μM. The increasingly stronger conversions of Form I to Form II and then Form III of DNA are observed with the increase of concentration of N-EoCen, with the total disappearance of the plasmid form at the 28.6 μM for apoN-EoCen and 2.86 μM for holoN-EoCen. In other words, among range of experiments concentration, the cleavage of holoN-EoCen to DNA is the stronger one. Interestingly, it is can be found that holoN-EoCen can promote the formation of Form II DNA in contrast with apoN-EoCen, which exhibits facilitation to conversion from From I to From III.

3.2.2 Kinetic of DNA cleavage by N-EoCen. The kinetic parameters in regard to the ability of N-EoCen to cleave DNA were calculated by following the time dependence of the reaction under the same conditions (Fig. 5D and E). The loss of DNA of Form I and increased levels of Form II and Form III were quantified after gel electrophoresis, and then fitted with the aid of the single-exponential fitting procedures (Fig. 5F). The reaction profile of DNA cleavage for the loss of From I displays first-order kinetic behavior, with $k = (0.0130 \pm 0.0010)$ min^{-1} of apoN-EoCen, and (0.0220 ± 0.0020) min^{-1} of holoN-EoCen. The data clearly represent that holoN-EoCen cleaves the DNA more quickly under the experimental conditions, namely the apoN-EoCen is relatively slower. Note that the products are mainly the From II of DNA for the holoN-EoCen, in comparision with apoN-EoCen, which primarily generates Form III of DNA over time. The results may be caused by the conformational change of holoN-EoCen, which can contribute to the cleavage of DNA. On the other hand, the complexation of Ca(II) with protein possibly favors the ionization of neighboring residues by Ca(II), potentially affecting the process.[57,58] Besides, apart from the part of coordination with protein, the excess Ca(II) also can bind with DNA. Therefore, the distance between the scissile phosphates shorten in the presence of Ca(II),[10] which is also favour of the cleavage. But there is a need to further research why the different products are produced by proteins.

3.3 DNA cleavage mechanism

As for the functional amino acids in the cleavage process, there are various opinions. Steitz TA and Shulman RG thought of that Ser plays critical roles in the enzyme activity of serine proteases.[59] Furthermore, the works by Zhao Yufen and coworkers[60,61] have shown that the cleavage of the dipeptide serine histidine (SH) to DNA is referred to the hydroxyl group in Ser. The
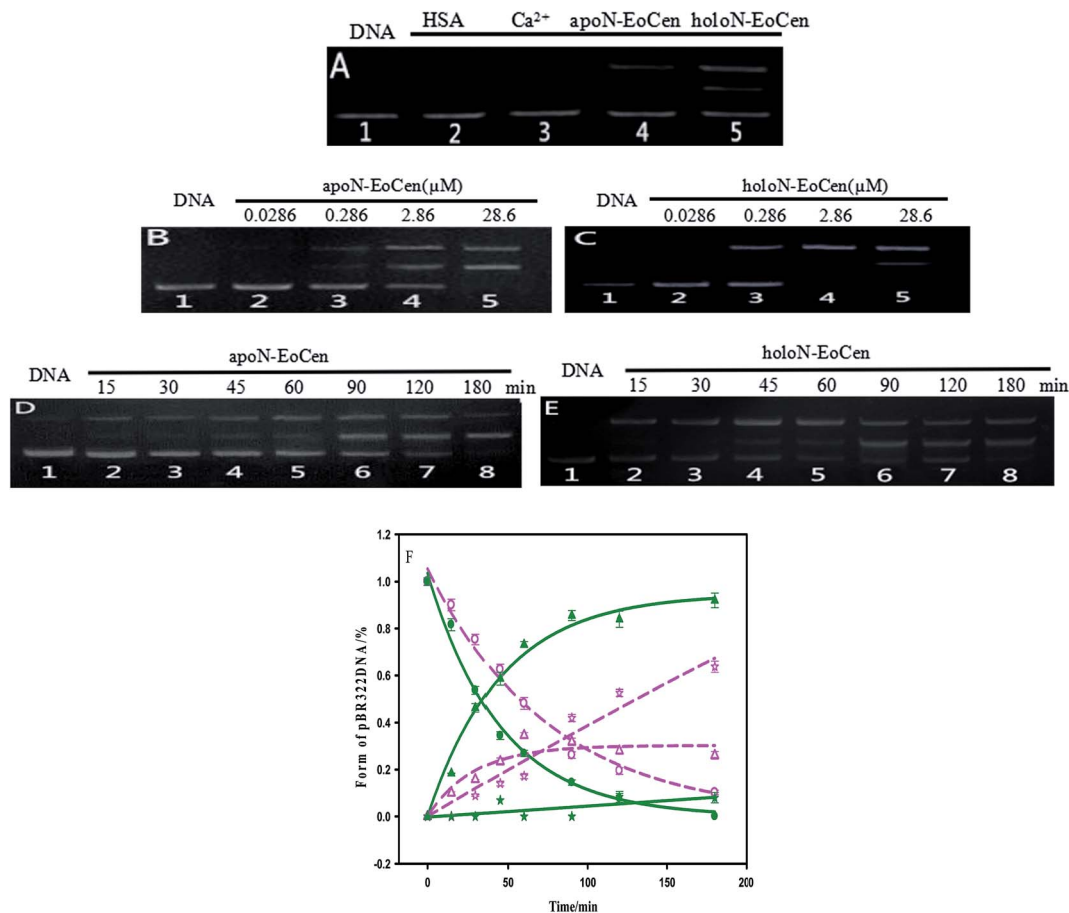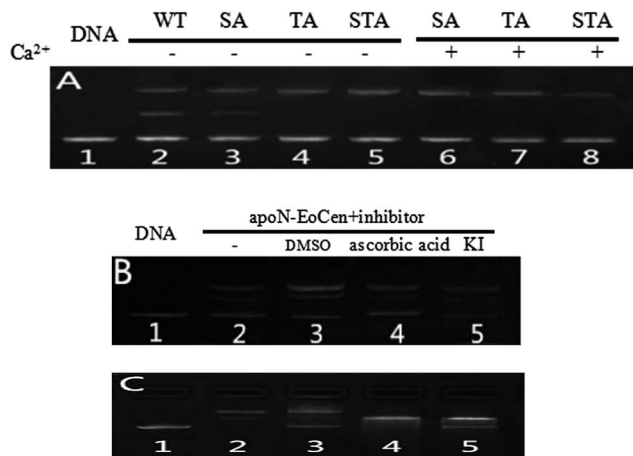
Fig. 5 Agarose gel electrophoresis of pBR322 DNA (0.025 μg μL^{-1}) after incubation with different species for 2 h in 10 mM Hepes buffer (pH 7.4) at room temperature (A). Lane 1 control untreated supercoiled DNA, lane 2 HSA + DNA, lane 3 Ca^{2+} + DNA, lane 4 apoN-EoCen + DNA, lane 5 holoN-EoCen + DNA, [Ca^{2+}] = 2 mM, [protein] = 2.22 μM. Agarose gel electrophoresis of pBR322 DNA (0.025 μg μL^{-1}) after incubation with apoN-EoCen (B) or holoN-EoCen (C) with various concentrations (0.0286, 0.286, 2.86 and 28.6 μM) for 3 h corresponding to lane 2–5, line 1 control untreated plasmid DNA. Agarose gel electrophoresis of pBR322 DNA (0.025 μg μL^{-1}) after incubation with apoN-EoCen (2.86 μM) (D) or holoN-EoCen (2.86 μM) (E) for 0–180 min corresponding to lane 1–8. The plots of content of Form I (*empty circle represents apoN-EoCen and filled circle is holoN-EoCen*), Form II (*empty triangle represents apoN-EoCen and filled triangle is holoN-EoCen*) and Form III (*empty pentagram represents apoN-EoCen and filled pentagram is holoN-EoCen*) against time (F), data come from (D) and (E), pink, dark green lines are the fitting results according to single-exponential fitting procedures. Each assay was performed in three independent replicates, and values shown are means with SD.

replaced by Thr still has cleavage activity. An appropriate distance is the essential to the cleavage of protein to DNA, so that nucleophilic attack to phosphorus center occurs and a pentacoordinate phosphorus transition state is formed, ultimately DNA is cleaved.[60] Soon afterwards, they further verified that Ser is the necessary amino acid in the cleavage process by a QM-MM calculation method.[61] In addition, research referred to endonuclease puts forward that Ser and Thr are essential for DNA cleavage.[62] Interestingly, these amino acids are kept on in different endonuclease. Besides, the group of Lin Yingwu[63] believes that a distinct distal hydrogen-bonding network of L29E Mb is responsible for efficient DNA cleavage. In fact, N-EoCen has two Ser (position 22, 43) and three Thr (position 38, 41, 90). Among which, Thr located at 41 and Ser located at 43 take part in the coordination with Ca(II). Thus we speculate that the cleavage of DNA by N-EoCen observed here probably attributed to the hydroxyl group of Ser and Thr in protein, so

that the protein exhibits an excellent ability of double stranded DNA cleavage.

To speculate the possible amino acids in the cleavage process, the DNA cleavage activity of mutant proteins was evaluated using agarose gel electrophoresis assay. As shown in Fig. 6A, apoN-EoCen is found to effectively cleave double strand DNA, leading to the formation of ∼28% nicked circular and ∼22% linear DNA after 1 h incubation at room temperature (lane 2). Control experiment shows that no DNA cleavage takes place for untreated DNA alone (lane 1). More interestingly, only nicked circular DNA is formed by SA apoN-EoCen (lane 4) and STA apoN-EoCen (lane 5) under the same condition. TA apoN-EoCen also shows reduced cleavage activity, with a result of ∼27% nicked circular DNA and ∼12% linear DNA (lane 3). Surprisingly, Ca(II) loaded mutant proteins merely produce little nicked circular DNA (lane 6, 7, 8). Results reflect that Ser and Thr, in particular Ser, are crucial in DNA cleavage process.

Fig. 6 Agarose gel electrophoresis of pBR322 DNA (0.025 µg µL^{-1}) after incubation with different protein (2.44 µM) for 1 h incubation in 10 mM Hepes buffer (pH 7.4) at room temperature (A), lane 1 control untreated supercoiled DNA. Cleavage of pBR322 DNA (0.025 µg µL^{-1}) by apoN-EoCen (16.6 µM) after 2 h incubation in the presence of inhibitors (B), lane 1 control untreated supercoiled DNA, lane 2 DNA + apoN-EoCen, lane 3 DNA + DMSO (0.4 M) + apoN-EoCen, lane 4 DNA + ascorbic acid (0.4 M) + apoN-EoCen, lane 5 DNA + KI (10 mM) + apoN-EoCen. Agarose gel electrophoresis for ligation of pBR322 DNA cleavage products (C), lane 1 control untreated supercoiled DNA, lane 2 DNA + apoN-EoCen, lane 3 isolation DNA cleavage products after incubation with apoN-EoCen + T4 DNA-ligase, lane 4 DNA + BamH I, lane 5 isolation DNA cleavage products after incubation with BamH I + T4 DNA-ligase. The DNA cleavage products after reaction with BamHI or apoN-EoCen for 3 h were isolated with QIAquick Gel Extraction Kit and incubation with T4 DNA ligase at 16 °C for 15 h.

3.3.1 Inhibition studies.
In order to further clarify the mechanism of DNA cleavage by N-EoCen, the experiments using various inhibiting agents were carried out. Inhibitors usually used are hydroxyl radical scavengers (DMSO, KI), and superoxide scavenger (ascorbic acid).[64] As shown in Fig. 6B, the experiment results shows that the DMSO (lane 3), ascorbic acid (lane 4), KI (lane 5) do not show inhibition effect on DNA cleavage. Therefore, hydroxyl radical and superoxide should be rule out of the DNA cleavage reactions. And thus, the mechanism of cleavage by N-EoCen may be a hydrolysis mechanism under experiment condition, as confirmed in T4-ligase ligation experiments.

3.3.2 T4 ligation experiment.
Obvious evidence of DNA hydrolysis by N-EoCen came from T4-ligase ligation experiments. The DNA cleavage products produced by N-EoCen were isolated by electrophoresis and extracted using the DNA gel extraction kit. Then the isolated products were treated with T4 DNA ligase at 16 °C for 15 h. At the same time, the ligation reactions of DNA cleavage products by BamHI endonuclease were proceed for comparison. The ligation products are visible by agarose gel electrophoresis assay. As shown Fig. 6C, the isolated nicked circular and linear DNA products cleaved by apoN-EoCen can be religated (*lane 3, lower band*). Besides, the linear DNA has also been religated by T4 ligase (*lane 5, lower band*). Hence, the cleavage process of DNA by N-EoCen occurs *via* a hydrolytic path.

3.3.3 The crucial amino acid in the cleavage process.
In order to further evaluate the cleavage mechanism, kinetic parameters of mutant proteins were firstly measured by following the time dependence of the reaction under the same conditions. Fig. 7A and B shows the transformation of DNA from From I to From II and From III induced by different mutant proteins at Ca(II) depleted state. The loss of DNA of Form I and increased levels of Form II and Form III quantified and fitted were shown in Fig. 7C. Importantly, our experiments results show that the cleavage activity of mutant proteins is substantially low in comparison with apoN-EoCen, especially for SA apoN-EoCen ((0.0090 ± 0.0002) min^{-1}) and STA apoN-EoCen ((0.0071 ± 0.0001) min^{-1}). TA apoN-EoCen has minor kinetic parameter ((0.0110 ± 0.0003) min^{-1}) than that apoN-EoCen. Subsequently, DNA cleavage behaviors of Ca(II) binding mutant proteins were also monitored, as shown in Fig. 7B. The cleavage activities decrease dramatically and they only produce nicked circular DNA with less kinetic parameters ((0.0010 ± 0.0001) min^{-1} for TA holoN-EoCen and SA holoN-EoCen, (0.0008 ± 0.0001) min^{-1} for STA holoN-EoCen).

Results suggest that Ser and Thr of N-EoCen, in particular Ser, may be primarily responsible for DNA cleavage under these conditions. The hydroxyl group of Ser and Thr can nucleophilic attack to phosphorus center and results in DNA cleavage. Even though Ser located at 43 (Ser43) and Thr located at 41 (Thr41) in the first EF-hand loop take part in coordination with Ca(II), holoN-EoCen displays increasing cleavage activity. The activity may mainly derive from Ser22, Thr38 and Thr90, in particular Ser. Moreover, holoN-EoCen with more surface-exposed seems to be favour of the contact between these amino acids and DNA phosphorus center, further increasing the cleavage activity. Compared with apoN-EoCen, mutant proteins with partial exposure critical amino acid residues undoubtedly exhibit reduced rapidly cleavage activity. The minor cleavage activity of mutant proteins may have association with the large conformation change induced by mutant. As shown in Fig. 7D, the alteration in the local environment molecular composition of mutant proteins leads to large secondary structural change. A remarkable decrease of the signal at 222 nm of mutant proteins in CD spectra is observed, which suggests mutant proteins with less α-helix, particularly for STA N-EoCen. Such conformational dynamics changes may weaken the attack to phosphorus center by hydroxyl group of Ser and Thr. Apparently, the substitute of coordination amino acids by Ala can affect substantially Ca(II) binding. Perhaps, great conformation change of Ca(II) loaded mutant proteins may relate to the less endonuclease-like activity. Note that human serum albumin (HSA) also has Ser and Thr distribution on the surface of protein. Nevertheless, HSA exhibits no cleavage activity to DNA under the similar conditions, as shown in Fig. 5A. It seems that HSA cannot bind with DNA effectively. Thus HSA has no cleavage activity. It emphasizes the combination prior of cleavage is critical for the endonuclease-like activity of N-EoCen.

3.3.4 Hydrolysis activity of N-EoCen.
To further understand the contribution of functional amino acids to endonuclease-like of N-EoCen, 4NPA was used as a typical substrate to inspect
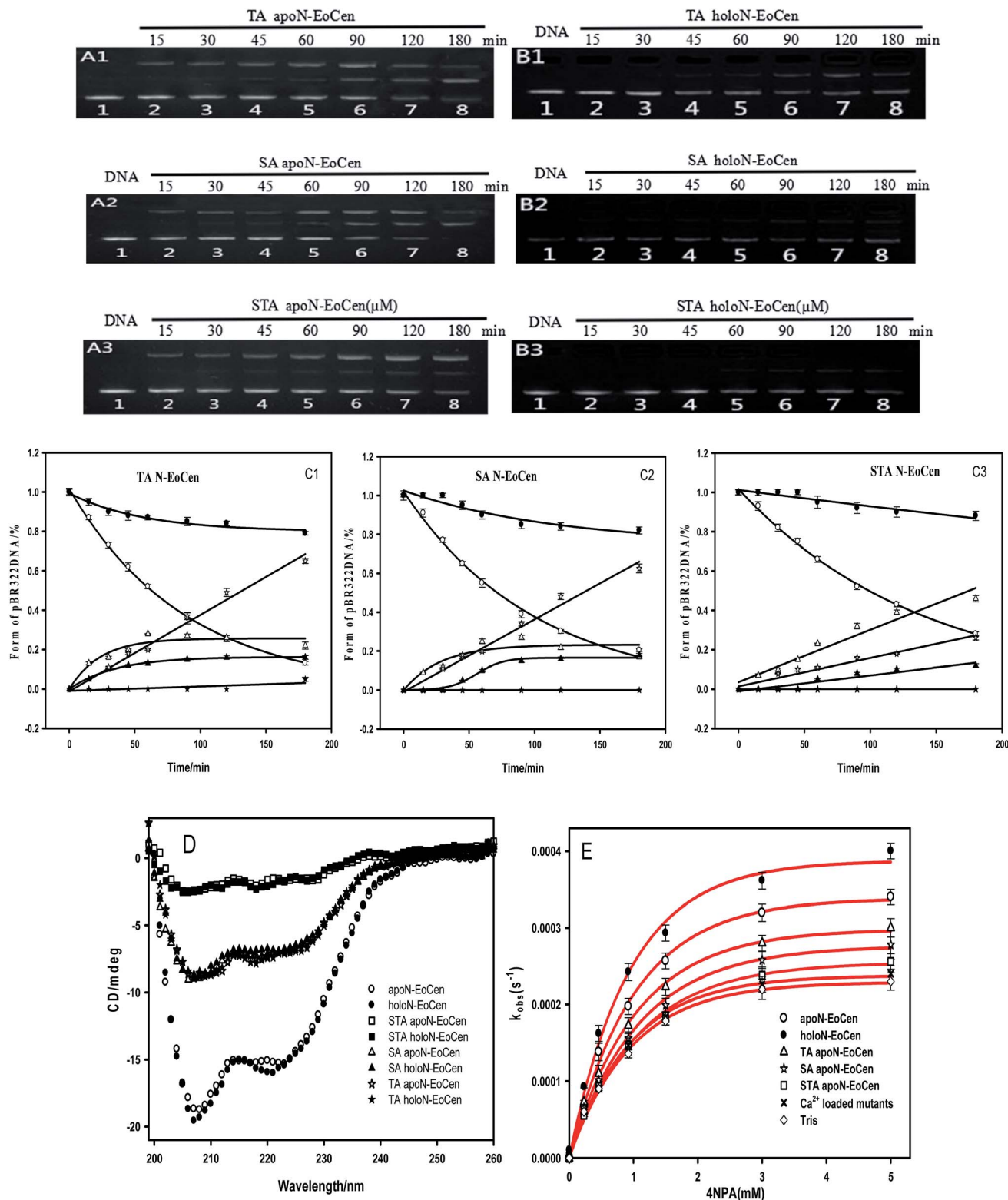
Fig. 7 Agarose gel electrophoresis of pBR322 DNA (0.025 μg μL⁻¹) after incubation with TA apoN-EoCen (A1), TA holoN-EoCen (B1), SA apoN-EoCen (A2), SA holoN-EoCen (B2), STA apoN-EoCen (A3) and STA holoN-EoCen (B3) for 0–180 min corresponding to lane 1–8. The plots of content of Form I (*empty circle represents apoprotein and filled circle is holoprotein*), Form II (*empty triangle represents apoprotein and filled triangle is holoprotein*) and Form III (*empty pentagram represents apoprotein and filled pentagram is holoprotein*) against time (C1, C2, C3), data come from (A and B). Conformational changes of mutant proteins and N-EoCen monitored by CD spectroscopy in 10 mM Hepes buffer (pH 7.4) at room temperature (D). Michaelis–Menten kinetics for the hydrolysis of 4NPA catalyzed by different proteins (5 μM protein in 10 mM Tris–HCl, pH 7.0, 25 °C) (E), apontaneous hydrolysis of 4NPA under the same condition was shown for comparison. Each assay was performed in three independent replicates, and values shown are means with SD.

closely the hydrolysis process.[34] As seen in Fig. S3,† the absorbance of 4-nitrophenoxide (hydrolysis product) at 400 nm gradually increases, suggesting 4NPA was hydrolyzed by apoN-EoCen. Shown in Fig. 7E is a plot of k_{obs} versus the concentration of 4NPA. Kinetic parameters, corrected of the spontaneous hydrolysis effect and yielded by a fit of the data to Michaelis–Menten equation, were summarized in Table 3. holoN-EoCen, with a k_{cat} value of $(4.75 \pm 0.08) \times 10^{-4} \text{ s}^{-1}$, represents relatively high catalysis hydrolysis activity to 4NPA than that of apoN-EoCen $((4.08 \pm 0.11) \times 10^{-4} \text{ s}^{-1})$. TA apoN-EoCen, SA apoN-EoCen and STA apoN-EoCen perform about 1.14-fold, 1.23-fold and 1.27-fold reduced catalysis hydrolysis activity compared to that of apoN-EoCen. Obviously, mutant proteins display lower catalysis hydrolysis activity. Upon Ca(ɪɪ) binding, the catalysis hydrolysis activity of mutant proteins intensively decreases. The obtained kinetic parameters for Ca(ɪɪ) loaded mutant proteins (SA holoN-EoCen, TA holoN-EoCen and STA holoN-EoCen) are about $(2.83 \pm 0.10) \times 10^{-4} \text{ s}^{-1}$, giving about 1.44-fold decrease than apoN-EoCen.

The results suggest that N-EoCen exactly performs catalytic hydrolysis activity, involving in Ser and Thr amino acid residues. Compared with apoN-EoCen, holoN-EoCen promotes whereas mutant proteins inhibit the catalytic hydrolysis of 4NPA. It is likely due to the fact that holoN-EoCen with open conformation as well as several Ser and Thr located at the protein surface may regulate the accessible volume for the substrate. In the hydrolysis process, Ser residue may play much more role than Thr residue. Additionally, Ca(ɪɪ) loaded mutant proteins show less hydrolysis activity than Ca(ɪɪ) depleted state mutant proteins. It seems that the mutant proteins with variational conformation further render the active amino acids inaccessible to substrate.

On the other hand, the K_m values of different proteins indicate that both Ca(ɪɪ) depleted and loaded mutant proteins have a lower affinity to the substrate of 4NPA. Based on the k_{cat} and K_m values, apoN-EoCen and holoN-EoCen show overall catalytic activity (k_{cat}/K_m) of 0.45 $\text{M}^{-1} \text{ s}^{-1}$ and 0.52 $\text{M}^{-1} \text{ s}^{-1}$, respectively. Meanwhile, TA apoN-EoCen, SA apoN-EoCen, and STA apoN-EoCen show gradually decreasing catalytic hydrolysis activity (Table 3). Ca(ɪɪ) binding mutant proteins only exhibit minor catalytic efficiency than mutant proteins.

Further support for the view comes from the close inspection of protein structure, providing possible reasons why holoN-

EoCen has relative high hydrolysis activity than others. Fig. 8A displays sequence alignments of apoN-EoCen and various mutant proteins. Blue and red shading represent potential Ca(ɪɪ) coordinating residues and mutant amino acids, respectively. Fig. 8B shows the coordination environment of both Ca(ɪɪ) binding loop of EF-hand of N-EoCen vividly. Thr41 and Ser43 residues of the functional Ca(ɪɪ) binding loop I are substituted by Ala, leading to the Ca(ɪɪ)-binding capacity decrease. Moreover, a computational molecular model of holoN-EoCen structure was built using the SwissModel server (DOI: 10.1093/nar/gku340)[65] with default parameters to compare with apoN-EoCen (PDB:2joj). The best template, a mouse centrin 1, was used to build the model. They share a high sequence identity of 56.16%. A detailed comparison of apoN-EoCen with holoN-EoCen structure shows in Fig. 8C. It clearly shows that holoN-EoCen with open conformation displays large differences consisting of the important inter-helical angles and Ca(ɪɪ) binding loops. Additionally, the critical amino acid residues involved in the cleavage to DNA are slight difference with those of apoN-EoCen, except Ser located at 22 (Ser22). Significantly, Ser22 clearly points towards inside upon Ca(ɪɪ) binding, which may constitute the foundation of major hydrolysis activity.

Based on obtained experiment results, a speculated schematic representation the interaction of N-EoCen with CT-DNA by ZDOCK 3.0.2 are presented on Fig. 8C. Usually, helix-loop-helix proteins can recognize specific DNA sequences by its helix, which is the most common protein structural element.[66] Taking into account the structure feature, it is presumable that N-EoCen inserts into the groove with its F-helix portion of EF-hand II embedded more deeply. holoN-EoCen populated open conformation triggers Ser22 more be accessible to the phosphorus center, favoring the hydrolysis to occur. Hence, Ser22 may play significant role in the endonuclease-like activity of N-EoCen. In contrast, mutant proteins with less α-helix may react with DNA in another way. Due to partial exposure of critical amino acids and less α-helix, mutant proteins perform little hydrolysis activity. With regard to Ca(ɪɪ) binding mutant proteins with markedly reduced activity, the most reasonable explain may be linked to the presence of a large conformation variation.

Finally, a plausible mechanism is shown in Fig. 8D, hydroxyl group of Ser and Thr nucleophilic attacks to phosphorus center, resulting in the formation of a pentacoordinate phosphorus transition state and efficient DNA cleavage taking place.

In addition to the description of the bulk of cellular centriole-related functions of centrin, cell fractionation experiments have positioned it within the nucleus. As for the functions within the nucleus, it has been found that centrin participates in the recognition process of NER. NER is a complicated process involved in much steps and more than thirty proteins. It is well known that centrin can stimulate NER activity in vitro by interacting directly with XPC in cooperation with human homologue of HR23B. However, the research about centrin-DNA direct interactions remain lacking. Some proteins, similarly to centrin and belonging to the members of calmodulin superfamily, can interact with specific sequence in DNA.[67] Literature has found the existence of interactions between

Table 3 Kinetic parameters of 4NPA hydrolysis catalyzed by different protein

| Protein	k_{cat} ($\text{s}^{-1} \times 10^{-4}$)	K_m (mM)	k_{cat}/K_m ($\text{M}^{-1} \text{ s}^{-1}$)
apoN-EoCen	4.08 ± 0.11	0.91 ± 0.05	0.45
TA apoN-EoCen	3.58 ± 0.12	0.95 ± 0.05	0.38
SA apoN-EoCen	3.33 ± 0.10	0.99 ± 0.06	0.34
STA apoN-EoCen	3.22 ± 0.08	0.99 ± 0.05	0.33
holoN-EoCen	4.75 ± 0.08	0.92 ± 0.03	0.52
TA holoN-EoCen	2.83 ± 0.10	0.88 ± 0.06	0.32
SA holoN-EoCen	2.83 ± 0.10	0.88 ± 0.06	0.32
STA holoN-EoCen	2.83 ± 0.10	0.88 ± 0.06	0.32

A

	E-helix	EF-hand I	F-helix
N-EoCen	ELSEEQKQEIKEAFDLF	**D T N K T G S I D Y H E**	LKVAMRAL
SA EoCen	ELAEEQKQEIKEAFDLF	**D T N K T G A I D Y H E**	LKVAMRAL
TA EoCen	ELSEEQKQEIKEAFDLF	**D A N K A G S I D Y H E**	LKVAMRAL
STA EoCen	ELAEEQKQEIKEAFDLF	**D A N K A G A I D Y H E**	LKVAMRAL

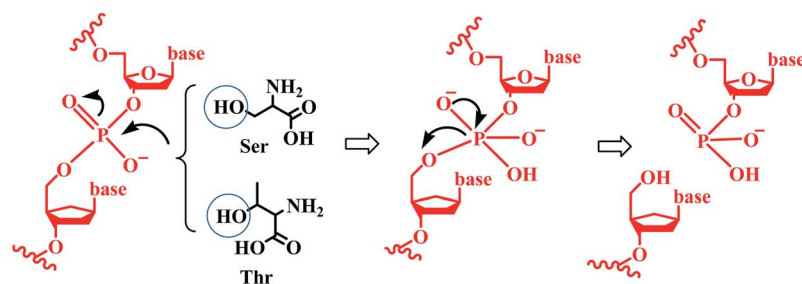|	E-helix	EF-hand II	F-helix
N-EoCen	GFDVKKPEILELMNEY	**D R E G N G Y I G F D D**	FLDIMTEK
SA EoCen	GFDVKKPEILELMNEY	**D R E G N G Y I G F D D**	FLDIMTEK
TA EoCen	GFDVKKPEILELMNEY	**D R E G N G Y I G F D D**	FLDIMAEK
STA EoCen	GFDVKKPEILELMNEY	**D R E G N G Y I G F D D**	FLDIMAEK

B
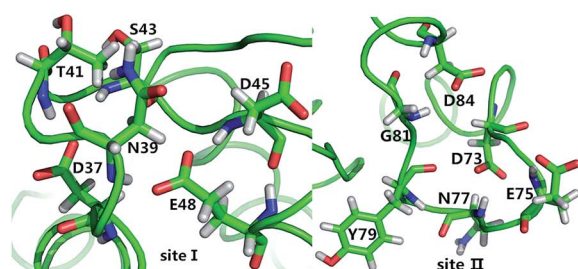
C
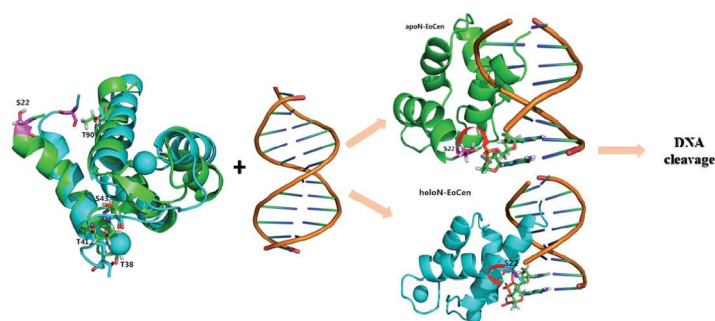
D

Fig. 8 Schematic representation the interaction of apoN-EoCen (PDB:2joj, green) and modelled holoN-EoCen (cyan) with CT-DNA. (A) Sequence alignments of N-EoCen and various mutant proteins. Blue and red shading represent potential Ca^{2+} coordinating residues and mutant amino acids, respectively. (B) Structural models of the Ca^{2+} binding loops I and II for the N-EoCen. Amino acids are numbered according to their position. D stands for aspartate, N for asparagine, T for threonine, S for serine, E for glutamate, Y for tyrosine, G for glycine. (C) Schematic representation the interaction of apoN-EoCen and modeled holoN-EoCen with CT-DNA by ZDOCK 3.0.2. S and T are shown as stickmodels (S22 is in pink sticks). The coordinated Ca^{2+} is shown as a cyan sphere. HoloN-EoCen structure was obtained by using the SwissModel server with default parameters based on best template. N-EoCen may be inserted into the groove with its α-helix portion and cleavage is proceeded. (D) Proposed mechanism for hydrolytic DNA cleavage by key amino acid residues.

centrin and DNA, which can result in abolishment of stimulation.[68] Based on the reported literature, the binding and cleavage activity of centrin to DNA represented currently may link to the functions within nucleus or NER. The activity may be enhanced in the presence of XPC. The research provides clues for further work. However, much more work remain needs to be done because it is unclear for the precise roles of centrin played in the process.

4 Conclusion

In summary, N-EoCen has been found to exhibit unusual affinity to double stranded DNA. The binding constants of holoN-EoCen and DNA are higher than that of apoN-EoCen under the same condition. The interaction profile probably may be that one protein molecular bind with one DNA molecular involved in about 35 bp. The binding of protein to the helix is entirely controlled by entropy change. Ultimately, the helix structure of DNA is subjected to perturbation. Meanwhile, the protein secondary structure as well as the Tyr environment changes to a large extent. More interestingly, N-EoCen exhibits endonuclease-like activity to DNA *via* a hydrolysis pathway. Ser and Thr, in particular Ser22, may be primarily responsible for DNA cleavage under these conditions. The flexibility of Ser located at 22 of EF-hand domains may explain the differences in cleavage activity between apoN-EoCen and holoN-EoCen. Note that the cleavage products are mainly nicked circular DNA for holoN-EoCen and linear DNA for apoN-EoCen, respectively. To date, there has been no evidence for the biochemical role of N-EoCen–DNA reaction. It is possible to relate to the cellular function of the protein in NER. The results on the protein–DNA interaction may find its future importance in the investigation of centrin more features.

Conflicts of interest

There are no conflicts to declare.

Acknowledgements

References

1 F. J. Blanco and G. Montoya, *FEBS J.*, 2011, **278**, 1643–1650.

2 D. Vuzman and Y. Levy, *Mol. BioSyst.*, 2012, **8**, 47–57.

3 B. Dey, S. Thukral, S. Krishnan, M. Chakrobarty, S. Gupta, C. Manghani and V. Rani, *Mol. Cell. Biochem.*, 2012, **365**, 279–299.

4 X. M. Ding, X. Y. Pan, C. Xu and H. B. Shen, *Curr. Comput.-Aided Drug Des.*, 2010, **6**, 197–206.

5 B. Y. Jiang, M. Wang, F. Z. Li, L. Yu and J. Q. Xie, *Biosens. Bioelectron.*, 2015, **64**, 429–433.

6 A. D. Robison and I. J. Finkelstein, *FEBS Lett.*, 2014, **588**, 3539–3546.

7 N. M. Luscombe, R. A. Laskowski and J. M. Thornton, *Nucleic Acids Res.*, 2001, **29**, 2860–2874.

8 N. R. Steffen, S. D. Murphy, L. Tolleri, G. W. Hatfield and R. H. Lathrop, *Bioinformatics*, 2002, **18**, S22–S30.

9 S. E. Halford and J. F. Marko, *Nucleic Acids Res.*, 2004, **32**, 3040–3052.

10 R. Molina, P. Redondo, S. Stella, M. Marenchino, M. D'Abramo, F. L. Gervasio, J. C. Epinat, J. Valton, S. Grizot, P. Duchateau, J. Prieto and G. Montoya, *Nucleic Acids Res.*, 2012, **40**, 6936–6945.

11 Z. Q. Deng, Q. Wang, Z. Liu, M. F. Zhang, A. C. D. Machado, T. P. Chiu, C. Feng, Q. Zhang, L. Yu, L. Qi, J. G. Zheng, X. Wang, X. M. Huo, X. X. Qi, X. R. Li, W. Wu, R. Rohs, Y. Li and Z. Z. Chen, *Nat. Commun.*, 2015, **6**, 7462.

12 L. Jen-Jacobson, *Biopolymers*, 1997, **44**, 153–180.

13 S. S. Narayanan and S. K. Pal, *Langmuir*, 2007, **23**, 6712–6718.

14 R. Errabolu, M. A. Sanders and J. L. Salisbury, *J. Cell Sci.*, 1994, **107**, 9–16.

15 T. Fischer, S. Rodriguez-Navarro, G. Pereira, A. Racz, E. Schiebel and E. Hurt, *Nat. Cell Biol.*, 2004, **6**, 840–848.

16 K. K. Resendes, B. A. Rasala and A. D. J. Forbes, *Mol. Cell. Biol.*, 2008, **28**, 1755–1769.

17 L. Radu, I. Durussel, L. Assairi, Y. Blouquit, S. Miron, J. A. Cox and C. T. Craescu, *Biochemistry*, 2010, **49**, 4383–4394.

18 T. J. Dantas, O. M. Daly, P. C. Conroy, M. Tomas, Y. Wang, P. Lalor, P. Dockery, E. Ferrando-May and C. G. Morrison, *PLoS One*, 2013, **8**, e68487.

19 T. J. Dantas, O. M. Daly and C. G. Morrison, *Cell. Mol. Life Sci.*, 2012, **69**, 2979–2997.

20 A. Paoletti, M. Moudjou, M. Paintrand, J. L. Salisbury and M. Bornens, *J. Cell Sci.*, 1996, **109**, 3089–3102.

21 L. Liang, S. Flury, V. Kalck, B. Hohn and J. Molinier, *Plant Mol. Biol.*, 2006, **61**, 345–356.

22 T. J. Dantas, Y. Wang, P. Lalor, P. Dockery and C. G. Morrison, *J. Cell Biol.*, 2011, **193**, 307–318.

23 M. Araki, C. Masutani, M. Takemura, A. Uchida, K. Sugasawa, J. Kondoh, Y. Ohkuma and F. Hanaoka, *J. Biol. Chem.*, 2001, **276**, 18665–18672.

24 R. Nishi, W. Sakai, D. Tone, F. Hanaoka and K. Sugasawa, *Nucleic Acids Res.*, 2013, **41**, 6917–6929.

25 E. X. Shi, W. L. Zhang, Y. Q. Zhao and B. S. Yang, *RSC Adv.*, 2017, **7**, 27139–27149.

26 M. R. Beccia, S. S. Merle, D. Lemaire, N. Brémond, R. Pardoux, S. Blangy, P. Guilbaud and C. Berthomieu, *J. Biol. Inorg. Chem.*, 2015, **20**, 905–919.

27 L. X. Ren, Y. Q. Zhao, J. Y. Feng, X. J. He, A. H. Liang and B. S. Yang, *Chin. J. Inorg. Chem.*, 2006, **22**, 87–90.

28 W. Liu, L. Duan, Y. Q. Zhao, A. H. Liang and B. S. Yang, *Chin. Sci. Bull.*, 2010, **55**, 3118–3122.

29 J. Marmur, *J. Mol. Biol.*, 1961, **3**, 208–218.

30 Z. Song, J. Ming and B. S. Yang, *J. Biol. Inorg. Chem.*, 2014, **19**, 359–374.

31 Z. Song, J. L. Wang and B. S. Yang, *Spectrochim. Acta, Part A*, 2014, **118**, 454–460.

32 J. R. Lakowicz, *Principles of fluorescence spectroscopy*, Kluwer Academic/Plenum, 1983, pp. 260–265.

33 B. S. Der, D. R. Edwards and B. Kuhlman, *Biochemistry*, 2012, **51**, 3933–3940.

34 J. Zeng, Y. Zhao, W. Li, X. S. Tan, G. B. Wen and Y. W. Lin, *J. Mol. Catal. B: Enzym.*, 2015, **111**, 9–15.

35 F. J. Kezdy and M. L. Bender, *Biochemistry*, 1962, **1**, 1097–1106.

36 W. W. Cleland, *Biochim. Biophys. Acta*, 1965, **67**, 104–137.

37 B. G. Pierce, K. Wiehe, H. Hwang, B. H. Kim, T. Vreven and Z. Weng, *Bioinformatics*, 2014, **30**, 1771–1773.

38 B. G. Pierce, Y. Hourai and Z. Weng, *PLoS One*, 2011, **6**, e24657.

39 J. Mintseris, B. Pierce, K. Wiehe, R. Anderson, R. Chen and Z. Weng, *Proteins*, 2007, **69**, 511–520.

40 N. J. Greenfield, *Nat. Protoc.*, 2006, **1**, 2876–2890.

41 J. Kypr, L. Kejnovska, D. Renciuk and M. Vorlickova, *Nucleic Acids Res.*, 2009, **37**, 1713–1725.

42 Z. J. Wang, Y. Q. Zhao, L. X. Ren, G. T. Li, A. H. Liang and B. S. Yang, *J. Photochem. Photobiol., A*, 2007, **186**, 178–186.

43 L. Duan, W. Liu, Z. J. Wang, A. H. Liang and B. S. Yang, *J. Biol. Inorg Chem.*, 2010, **15**, 995–1007.

44 Y. Q. Zhao, L. Song, A. H. Liang and B. S. Yang, *J. Photochem. Photobiol., B*, 2009, **95**, 26–32.

45 M. Zhangh, T. Tanaka and M. Ikura, *Nat. Struct. Mol. Biol.*, 1995, **2**, 758–767.

46 Y. Q. Zhao, J. Y. Feng, A. H. Liang and B. S. Yang, *Spectrochim. Acta, Part A*, 2009, **71**, 1756–1761.

47 W. O. Mcclure and G. M. Edelman, *Biochemistry*, 1966, **5**, 1908–1919.

48 Z. J. Wang, L. X. Ren, Y. Q. Zhao, G. T. Li, L. Duan, A. H. Liang and B. S Yang, *Spectrochim. Acta, Part A*, 2008, **70**, 892–897.

49 T. R. Prytkova, E. Ibrahim, S. Brian, N. Son-Binh and G. C. Schatz, *J. Phys. Chem. B*, 2010, **114**, 2627–2634.

50 A. Y. Solovyev, S. I. Tarnovskaya, I. A. Chernova, L. K. Shataeva and Y. A. Skorik, *Int. J. Biol. Macromol.*, 2015, **78**, 39–45.

51 L. Mcfail-Isom, C. C. Sines and L. D. Williams, *Curr. Opin. Struct. Biol.*, 1999, **9**, 298–304.

52 A. Sigel, H. Sigel and R. K. O. Sigel, *Interplay between metal ions and nucleic acids*, Springer, 2012, vol. 10, p. 38.

53 W. Chen, N. J. Turro and D. A. Tomalia, *Langmuir*, 2000, **16**, 15–19.

54 M. Voicescu, M. Heinrich and P. Hellwig, *J. Fluoresc.*, 2008, **19**, 257–266.

55 J. Eisinger, M. Gueron, R. G. Shulman and T. Yamane, *Proc. Natl. Acad. Sci. U. S. A.*, 1966, **55**, 1015–1020.

56 S. A. Coulocheri, D. G. Pigis, K. A. Papavassiliou and A. G. Papavassiliou, *Biochimie*, 2007, **89**, 1291–1303.

57 I. V. Korendovych, D. W. Kulp, Y. Wu, H. Cheng, H. Roder and W. F. DeGrado, *Proc. Natl. Acad. Sci. U. S. A.*, 2011, **108**, 6823–6827.

58 S. W. Wong-Deyrup, C. Prasannan, C. M. Dupureur and S. J. Franklin, *J. Biol. Inorg Chem.*, 2011, **17**, 387–398.

59 T. A. Steitz and R. G. Shulman, *Annu. Rev. Biophys. Bioeng.*, 1982, **11**, 419–444.

60 Y. F. Li, Y. W. Sha, Y. Ma and Y. F. Zhao, *Biochem. Biophys. Res. Commun.*, 1995, **213**, 875–880.

61 R. G. Zhong, L. J. Zhao and Y. F. Zhao, *Acta Chim. Sin.*, 2004, **62**, 2444–2446.

62 J. Prieto, P. Redondo, D. Padro, S. Arnould, J. C. Epinat, F. Paques, F. J. Blanco and G. Montoya, *Nucleic Acids Res.*, 2007, **35**, 3262–3271.

63 Y. Zhao, K. J. Du, S. Q. Gao, B. He, X. S. Tan and Y. W. Lin, *J. Inorg. Biochem.*, 2016, **156**, 113–121.

64 M. S. Deshpande, S. Junedi, H. Prakash, S. Nagao, M. Yamanaka and S. Hirota, *Chem. Commun.*, 2014, **50**, 15034–15036.

65 K. Arnold, L. Bordoli, J. Kopp and T. Schwede, *Bioinformatics*, 2006, **22**, 195–201.

66 C. W. Garvie and C. Wolberger, *Mol. Cell*, 2001, **8**, 937–946.

67 R. Kushwaha, A. Singh and S. Chattopadhyay, *Plant Cell*, 2008, **20**, 1747–1759.

68 Y. S. Krasikova, N. I. Rechkunova, E. A. Maltseva, C. T. Craescu and O. I. Lavrik, *Biochemistry*, 2012, 77, 346–353.